MDPI

Path-Following Formation of Fixed-Wing UAVs under Communication Delay: A Vector Field Approach

Thiem V. Pham [1,*] **and Thanh Dong Nguyen** [2]

1   Faculty of Electrical and Electronic Engineering, PHENIKAA University, Yen Nghia, Ha Dong,
    Hanoi 12116, Vietnam
2   Viettel High Technology Industries Corporation, Hanoi 12116, Vietnam; dongnt11@viettel.com.vn
*   Correspondence: thiem.phamvan@phenikaa-uni.edu.vn

Abstract: In many applications, such as atmospheric observation or disaster monitoring, cooperative control of a fleet of UAVs is crucial because it is effective in repeated tasks. In this work, we provide a workable and useful cooperative guiding algorithm for several fixed-wing UAVs to construct a path-following formation with communication delays. The two primary components of our concept are path-following (*lateral guidance*) and path formation (*longitudinal guidance*). The former is in charge of ensuring that, in the presence of wind disturbance, the lateral distance between the UAV and its targeted path converges using a well-known vector field technique. In the event of a communication delay, the latter ensures that several fixed-wing UAVs will create a predetermined formation shape. Furthermore, we provide a maximum delay bound that is dependent on the topology and a controller's gain. Lastly, in order to confirm the viability and advantages of our suggested approach, we construct an effective platform for a hardware-in-the-loop (HIL) test.

Keywords: communication delays; vector field; cooperation control; fixed-wing UAV; path-following formation

1. Introduction

The coordination of multi-unmanned aerial vehicle development has garnered significant attention in recent years. In both civil and military applications, they offer appealing benefits [1–3]. Unlike multi-rotor UAVs or ground vehicles, fixed-wing UAVs can only move forward at a minimum speed that produces enough lift to maintain their aerial position. They are unable to move backward. It should be noted that current methods (e.g., [4]) cannot address the significantly different performance of coordinated path-following control when there is a minimum forward speed constraint. One of the most important tasks in cooperative flight is path-following formation for the coordination of multiple fixed-wing UAVs. This task focuses on managing a group of fixed-wing UAVs flying along prearranged or planned paths while generating a desired formation pattern based on local interactions. Moreover, wind velocities typically range between 20% and 60% of the target velocity [5,6]. Consequently, effective path-following formation approaches are needed to handle this ongoing disturbance.

The path-following controller and coordinated control architecture must be integrated to accomplish coordinated path-following. Coordinated path-following control of multi-rotor UAVs [7–9] and ground vehicles [10,11] has been the subject of numerous studies. However, the majority of these results do not apply to fixed-wing UAVs due to the minimum forward speed restrictions, which severely limit the missions that can be accomplished with this class of vehicles. Recently, in [12,13], researchers explored the multiple-input multiple-output (MIMO) stochastic channel model for UAV-to-ground communication and anti-jamming trajectory design to ensure successful data collection. This model helps reduce the UAV's flight energy consumption within a finite task duration by concurrently optimizing the collection sequence of the sensor nodes and the UAV's flight trajectory.

The underlying algorithms relied on the assumption that the fixed-wing UAV has a low-level control system. It provides a vector field technique-based kinematic model to the guidance layer. More accurately, Frew [14] further refined it to phase keeping and to standoff tracking, and Lawrence [15] first described the standoff coordination of several fixed-wing UAVs based on Lyapunov vector fields. This method focuses on a decoupled control structure that responds to phase angle keeping and standoff distance, with both speed and direction rate. Accordingly, the study [16] developed the phase-keeping idea further and suggested a variable airspeed controller that coordinates UAV swarms through information exchange. Note that in the case of a stationary target in the loiter circle without wind, these algorithms only provide cooperative flying, not formation flight. In any particular restrictions, such wind or a delayed communications link on the UAV, the cooperative path-following of UAV swarms cannot be reached.

In contrast with decoupled control structures, a guidance law for multi-fixed-wing UAV coordination utilizing the potential function approach is provided; this potential function generates the velocity field [17]. This concept ensures that during the flying of UAV swarms, fixed-wing UAV swarms will arrive at loitering formation without collision. Moreover, a sliding mode control combined with a Lyapunov vector field is employed to construct a decentralized cooperative stand-off line-of-sight tracking of UAV swarms [18]. By holding a predefined distance from the moving object, it establishes a consistent pattern. Despite these approaches' advancements, there are still a number of obstacles in the path-following formation problem. It is also important to note that constraints on velocity have only been partially taken into account in the coordinated path-following issues for fixed-wing UAVs. A time-critical coordinated path-following control issue was used in [19], where the coordination was related to the UAVs' capacity to avoid collisions. A cooperative path-following issue was proposed, along with its necessary conditions [20]. According to Wang et al. [21], the proposed algorithm has the capability of simultaneously directing a number of fixed-wing unmanned aerial vehicles (UAVs) along predetermined trajectories and destination points. In recent studies, researchers have explored the distributed control of formation maneuvers in multi-agent systems using complex Laplacian techniques, alongside addressing angle-constrained formation control problems within a Leader-First Follower sensing framework [22,23]. These methods offer the advantage of maintaining invariant inter-edge angles despite uniform translations, rotations, and scalings of the entire formation, as long as the sensing graph remains directed and non-triangulated. These researched techniques are difficult to implement in the presence of communication delays.

Inspired by the previously stated studies, the study examines the path-following guidance formation issue for UAV swarms during communication delays. The path-following and the cooperative path controllers are the two primary components of the control structure that we propose. The former utilizes a vector field method with respect to the lateral guiding law [15], which is responsible for ensuring that, in the presence of wind disturbance, the lateral distance between the UAV and its predefined path converges to zero. Furthermore, a second counterpart, known as the longitudinal guidance rule, can be used to coordinate many fixed-wing UAVs. It allows a fixed-wing UAV swarm to be reached at a predetermined formation. We provide, specifically, a sufficient condition for the stability of a system in the presence of communication delay. Additionally, we provide a communication delay upper bound that is influenced by the formation controller's gain and the UAVs' communication graph. As a consequence, our method is simpler to utilize and more flexible than the results in [24,25], and it also requires fewer calculations when using the autopilot of a UAV. Furthermore, our technique is more comprehensive than those in [17,18,24–26] because it takes into account real-world scenarios such communication delays. Then, we design a benchmark of UAV swarms, comprising three primary components: autopilot (AP) systems, decentralized communication network, and ground control system (GCS). In conclusion, we provide a hardware-in-the-loop test that is both robust and dependable for evaluating UAV swarms. This test includes VT-Link, an AP system, a GCS.

The remainder of the paper is organized in this manner: In Section 2, the path-following formation problem of multiple fixed-wing UAVs is explained. Our main results are displayed in Sections 3 and 4. To illustrate the proposed approaches, simulation results and a hardware-in-the-loop (HIL) test are included in Sections 5 and 6. The outcomes and more studies are finally presented in Section 7.

2. Problem Description

We assume that UAV$^{[i]}$ is equipped with an autopilot that is responsible for maintaining altitude stability (see Section 3.4 in [27]). The resulting first-order systems represent the following dynamics of UAV$^{[i]}$:

$$\dot{\psi}^{[i]} = \alpha(\psi_c^{[i]} - \psi^{[i]}) \tag{1}$$

where $\psi^{[i]}$ represents the UAV's heading angle, α is a known positive constant, and $\psi_c^{[i]}$ is the controller's command heading. In this case, i, a superscript sign, represents UAV i^{th}, where $i = 1, 2, \cdots, N$, and N is the number of UAVs.

In the vector-field approach [14], to counter the wind effect, the course angle $\chi^{[i]}$ is considered. The dynamics of $\psi^{[i]}$ and $\chi^{[i]}$ are similar to those of (1) since the only difference is the wind effect, that is,

$$\dot{\chi}^{[i]} = \alpha(\chi_c^{[i]} - \chi^{[i]}) \tag{2}$$

where a command course angle of UAV$^{[i]}$, $\chi_c^{[i]}$, is defined by the vector field.

Next, we assume that all UAVs maintain a constant altitude and consider a cooperative path-following problem where N spatial paths in 2-D space are defined as follows:

$$\{\mathcal{P}^{[i]} : p_d^{[i]} \in \mathbb{R}^2, i \in \mathcal{N}\} \tag{3}$$

where $\mathcal{N} = \{1, 2, \cdots, N\}$ indicates the set of UAVs; a generic position vector of the path i, $p_d^{[i]}$, is expressed in the inertial North–East frame. UAV$^{[i]}$ is allocated to a path $\mathcal{P}^{[i]}$ as depicted in Figure 1.

We investigate the situation shown in Figure 1, in which a fleet of UAVs fly on the space and are specified by their corresponding position $p^{[i]}, i = 1, 2, \cdots, 5$. The objective of our problem is that all UAVs need to maneuver with the designed speed $V_a^{[i]}, i = 1, 2, \cdots, 5$ and converge to and reach an intended formation (V-shaped formation in this case). In the meantime, they track to their predefined paths $\mathcal{P}_{line}^{[i]}, i = 1, 2, \cdots, 5$, also known as path-following. Moreover, UAV$^{[i]}$ considers both delayed information regarding the states of its neighbors and delayed access to information about its own state.

In the following, we will focus on longitudinal motion (see Figure 1), where coordination between UAVs is rendered possible by designing an airspeed of UAV$^{[i]}, i \in \mathcal{N}$. It depends on the longitudinal distance, which shows a distance between UAV$^{[i]}$ and its predefined path [28]. It notes that the UAVs' *node set* is denoted by $\mathcal{V} := \{1, \cdots, N\}$, while the *edge set*, which encodes the communication interactions between the UAVs, is denoted by $\mathcal{E} \subseteq (\mathcal{V} \times \mathcal{V})$. $\mathcal{N}_i := \{j \in \mathcal{V} : (i, j) \in \mathcal{E}, i \neq j\}$ is a set of UAV$^{[i]}$'s neighbors. For an undirected graph, $\mathcal{G} = \{\mathcal{V}, \mathcal{E}\}$ is used to represent it. Let $a_{(ij)}$ represent the elements of the adjacency matrix $\mathcal{A}$, which is defined as follows: $\mathcal{A} = [a_{(ij)}]$. In the case where $(j, i) \in \mathcal{E}$, $a_{(ij)} > 0$; in other cases, $a_{ij} = 0$. $L_{ii} = \sum_{j \neq i} a_{ij}; L_{(ij)} = -a_{ij}$ is the definition of the Laplacian matrix $\mathcal{L} = [L_{ij}] \in \mathbb{R}^{N \times N}$.
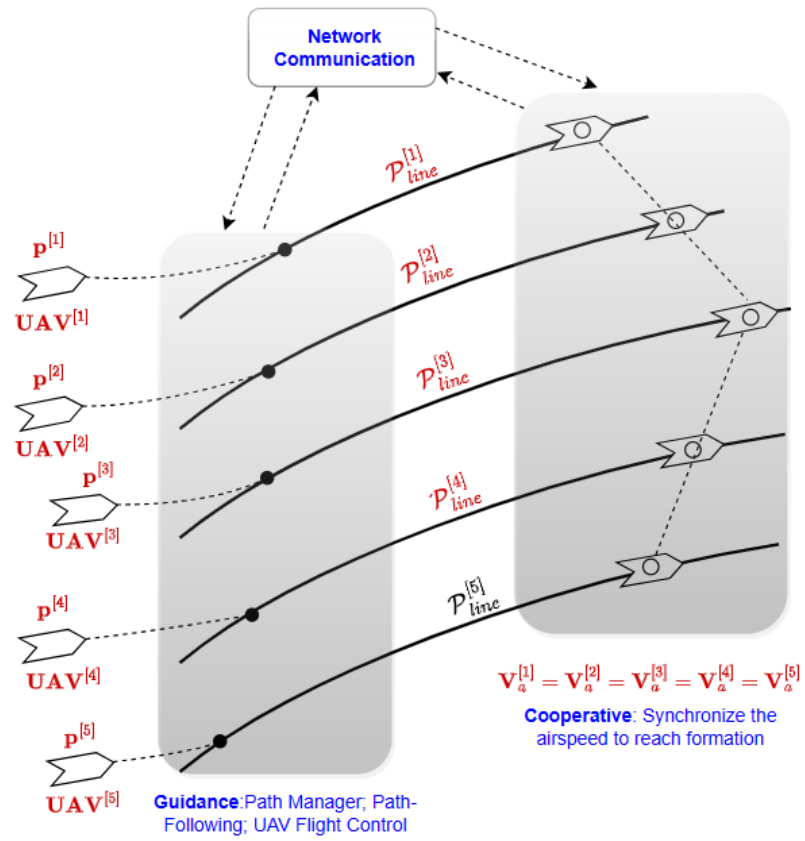
Figure 1. Illustrative proposed formation scheme of fixed-wing UAVs: A set of UAVs must converge to and maintain a desired geometric formation, and they follow their designated intended paths, or path-following.

2.1. Straight-Line Path-Following

A straight line is shown in Figure 2 with $p^{[i]} = [p_n^{[i]}, \ p_e^{[i]}] \in \mathbb{R}^2$.
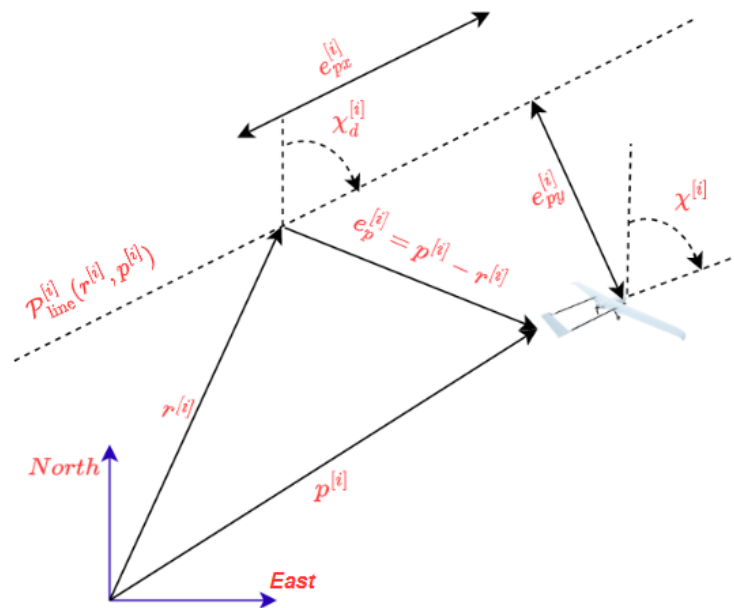
Figure 2. Illustrative straight line depicted by $\mathcal{P}_{line}^{[i]}(r^{[i]}, p^{[i]})$.

Let $\mathcal{R}_{\mathcal{I}}^{\mathcal{P}}$ be the transformation from the North–East inertial frame to the following path frame:

$$\mathcal{R}_{\mathcal{I}}^{\mathcal{P}} = \begin{bmatrix} \cos \chi_q^{[i]} & \sin \chi_q^{[i]} \\ -\sin \chi_q^{[i]} & \cos \chi_q^{[i]} \end{bmatrix} \tag{4}$$

where $\chi_q^{[i]} = \tan^{-1}(p_e^{[i]}, p_n^{[i]})$ is a course angle of $\mathcal{P}^{[i]}$ that is measured from the north, and let $e_p^{[i]} = [e_{px}^{[i]}, e_{px}^{[i]}]^T$ be the relative path error expressed in the path frame.

$$\begin{bmatrix} e_{px}^{[i]} \\ e_{py}^{[i]} \end{bmatrix} = \begin{bmatrix} \cos \chi_q^{[i]} & \sin \chi_q^{[i]} \\ -\sin \chi_q^{[i]} & \cos \chi_q^{[i]} \end{bmatrix} \begin{bmatrix} p_x^{[i]} - r_x^{[i]} \\ p_y^{[i]} - r_y^{[i]} \end{bmatrix} \tag{5}$$

2.2. Orbit Path-Following

For orbit path-following, the navigational dynamics can be conveniently changed to polar coordinates in term of $\rho^{[i]}$ and $\eta^{[i]}$. From Figure 3, the following can be seen:

$$p_x^{[i]} = p_{n\omega} + \rho^{[i]} \cos \eta^{[i]}$$
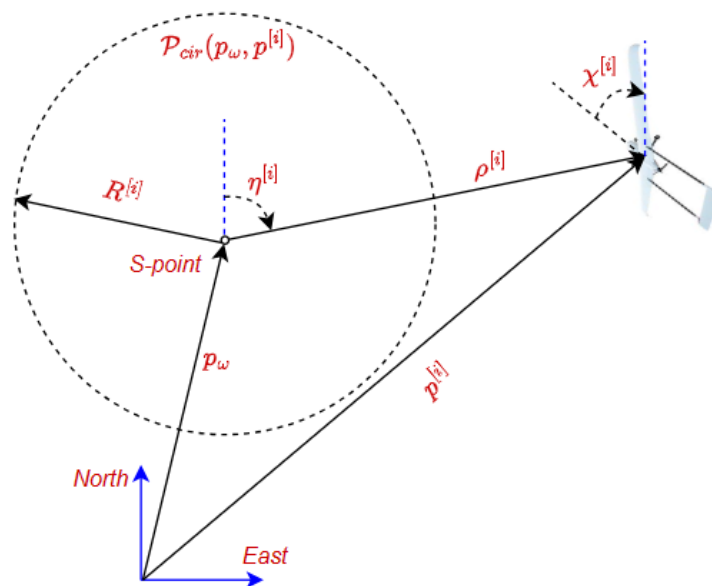$$p_y^{[i]} = p_{e\omega} + \rho^{[i]} \sin \eta^{[i]}$$

Figure 3. Orbit following indicated by $\mathcal{P}_{cir}^{[i]}(p_\omega, p^{[i]})$.

Taking the derivative, one has the equation of motion, which represents the UAV$^{[i]}$ motion to the following orbit $\mathcal{P}_{cir}^{[i]}$:

$$\begin{bmatrix} \dot{\rho}^{[i]} \\ \dot{\eta}^{[i]} \rho^{[i]} \end{bmatrix} = \begin{bmatrix} \cos \eta^{[i]} & \sin \eta^{[i]} \\ -\sin \eta^{[i]} & \cos \eta^{[i]} \end{bmatrix} \begin{bmatrix} \dot{p}_x^{[i]} - \dot{p}_{n\omega} \\ \dot{p}_y^{[i]} - \dot{p}_{e\omega} \end{bmatrix} \tag{6}$$

2.3. Problem Formulation

In this work, the path-following formation problem of UAV swarms will be rewritten as follows:

- Path-following problem: The lateral error between UAV$^{[i]}$ and its desired path $\mathcal{P}^{[i]}$ in (5) and (6) converges to zero, i.e.,

$$\lim_{t \to \infty} \left[\rho^{[i]}(t) - R^{[i]} \right] \to 0,$$

$$\lim_{t \to \infty} e_{py}^{[i]}(t) \to 0$$

- Path formation problem: Under the interaction between UAVs and time delays τ regarding their relative path errors in (5) and (6), their desired airspeed $V_a^{[i]}$ to reach the desired formation is determined.

$$\lim_{t \to \infty} [e_{px}^{[i]}(t - \tau) - e_{px}^{[j]}(t - \tau)] \to 0,$$

$$\lim_{t \to \infty} [\eta^{[i]}(t - \tau) - \eta^{[j]}(t - \tau)] \to 0$$

Consequently, in some cases, a trajectory intended for a UAV$^{[i]}$ flight can be approximately represented by combining different fundamental segments, including circular arcs and straight lines $\mathcal{P}^{[i]}$. For example, one can approximate the perimeter of any arbitrary geometric shape using a set of lines and arcs. Thus, without losing generality, this study examines the UAV path-following formation issue with a straight-line and circular path. Finally, we revisit the lemmas listed below.

Lemma 1 ([29]). *Since all eigenvalues $u_i = r_i + jw_i$, $j^2 = -1, i = 1, 2, \cdots, n$, of the matrix A satisfy the following requirements:*

- $w_i < 0$
- $h\sqrt{(r_i^2 + w_i^2)} < \tan^{-1}\left(\frac{|a_i|}{|b_i|}\right)$

The system $\dot{x}(t) = Ax(t - h)$, and $t \geq 0$ is asymptotically stable.

Lemma 2 ([30]). *Assuming that a graph is connected and undirected, $\mathcal{L}$ has simple zero eigenvalues, and other $N - 1$ eigenvalues have positive real parts. The appropriate right eigenvector is $\mathbf{1}_N$.*

3. Formation Straight-Line Path-Following under Communication Delay

As seen in Section 2.3, this section provides the solution for UAV swarm straight-line formation with delayed communication. Three components make up our method: constructing a straight line for N UAVs that ensures a safe spacing between UAVs and UAV trajectories that are parallel. The UAV is then required to follow the intended path by a lateral guidance law for path-following. Lastly, a proposed method with an upper restriction on the delay condition ensures that UAVs will reach a desired formation.

3.1. Definition of Straight Line

An objective of the defined paths $\mathcal{P}_{line}^{[i]}$ for UAVs is to be in parallel (see Figure 1). Particularly, this is based on four parameters: its desired formation, the path $r^{[i]}$'s root corresponding to the straight line, a UAV swarms' desired direction λ, and a desired course angle $\chi_d(\chi_q)$. The definition of a straight line for UAV$^{[i]}$ is constructed.

First, each UAV's straight line is calculated using the following (7):

$$r^{[i]} = r^l + \begin{bmatrix} \cos(\chi_d) & \sin(\chi_d) \\ -\sin(\chi_d) & \cos(\chi_d) \end{bmatrix} \Gamma^{[i]}, l \neq i = 1, 2 \cdots, N \tag{7}$$

where $\Gamma^{[i]}$ indicates the relative desired positions between UAVs and a leader, and r^l is the predefined UAV$^{[l]}$'s position, where UAV$^{[l]}$ is called leader with $l \neq i = 1, 2 \cdots, N$. A direction from a UAV leader to its waypoint (*which is defined by an operator*) is defined as χ_d. It notes here that the desired shape formation between UAVs is given as $\mathbf{\Gamma} = [\Gamma^{[1]}, \cdots, \Gamma^{[N]}]^T \in \mathbb{R}^2$.

Therefore, the defined paths $\mathcal{P}_{line}^{[i]}$, $i = 1, 2, \cdots, N$ for UAVs are constructed as follows:

$$\{\mathcal{P}_{line}^{[i]} : p^{[i]} \leftarrow r^{[i]} + \lambda[\cos(\chi_d) \ \sin(\chi_d)]\} \tag{8}$$

3.2. Lateral Guidance Law

As mentioned into Section 3.1, the design algorithm for UAV$^{[i]}$ is first examined; it follows $\mathcal{P}_{line}^{[i]}$, which is the intended path, in (8). Particularly, our proposed algorithm ensures that UAV$^{[i]}$ follows an accurately desired path $\mathcal{P}_{line}^{[i]}$ in (8) for UAV$^{[i]}$ in the presence of constant wind. Our objective is constructed as a vector field so that it is directed toward the predefined path. As a result, the demanded course, which is to drive UAV$^{[i]}$ on the path, is given as follows:

$$\chi_d^{[i]} = \chi_q - \chi_\infty \frac{2}{\pi} \tan^{-1}(k e_{py}^{[i]}) \tag{9}$$

where $e_{py}^{[i]}$ in (5), $\chi_\infty \in (0, \frac{\pi}{2}]$, k is a positive parameter.

To guarantee $\chi^{[i]} \to \chi_d^{[i]}$ and $e_{py}^{[i]} \to 0$ as $t \to 0$, Equation (10) gives a course angle, where $k_{sl} = \chi_\infty \frac{2k\|V_g\|}{\alpha\pi}$. Moreover, control aggressiveness is governed by ρ, α, which also mitigate any potential chattering in a control action.

$$\chi_c^{[i]} = \chi^{[i]} - \frac{k_{sl}}{1 + (k e_{py}^{[i]})^2} \sin\chi^{[i]} - \frac{\rho}{\alpha}\text{sgn}\left(\chi^{[i]} - \chi_d^{[i]}\right) \tag{10}$$

Let $\bar{\chi}^{[i]} = \chi^{[i]} - \chi_d^{[i]}$ and $e_{py}^{[i]}$ in (5); their dynamics can be described by using (2) and (9).

$$\begin{aligned} \dot{e}_{py}^{[i]} &= V_g^{[i]} \sin(\chi^{[i]} - \chi_q) \\ \dot{\chi}^{[i]} &= \alpha(\chi_c^{[i]} - \chi^{[i]}) + \chi_\infty \frac{2}{\pi} \frac{k}{1 + (k e_{py}^{[i]})^2} \dot{e}_{py}^{[i]} \end{aligned} \tag{11}$$

As a result, one has the following lemma:

Lemma 3. *The system (11) with $\chi_c^{[i]}$ is given in (10), which is asymptotically stable, which means the following:*

$$\lim_{t \to \infty} e_{py}^{[i]}(t) \to 0, \quad \lim_{t \to \infty} \bar{\chi}^{[i]}(t) \to 0$$

if $\chi_\infty \in (0, \frac{\pi}{2}]$ and $\frac{\rho}{V_g^{[i]}} \frac{4\chi_\infty k}{\pi} > 1$.

Proof. We consider the candidate Lyapunov function as follows:

$$V^{[i]} = \frac{1}{2}\left(e_{py}^{[i]}\right)^2 + \frac{1}{2}\left(\bar{\chi}^{[i]}\right)^2$$

A sufficient condition to guarantee (11) is that the derivative of a Lyapunov function is less than zero. Then, by taking the derivative of Lyapunov and using (11), one has the following:

$$\begin{aligned} \dot{V}^{[i]} &= e_{py}^{[i]}\dot{e}_{py}^{[i]} + \frac{1}{2}\bar{\chi}^{[i]}\dot{\bar{\chi}}^{[i]} \\ &= e_{py}^{[i]} V_g^{[i]} \sin(\chi^{[i]} - \chi_q) \\ &\quad + \bar{\chi}^{[i]}\alpha\left[(\chi_c^{[i]} - \chi^{[i]}) + \frac{1}{\alpha}\frac{2\chi_\infty}{\pi}\frac{k}{1 + (k e_{py}^{[i]})^2}\dot{e}_{py}^{[i]}\right] \end{aligned}$$

and utilizing (10) and (9), one has the following:

$$\dot{V}^{[i]} = e_{py}^{[i]} V_g^{[i]} \sin(\bar{\chi}^{[i]} - \chi_\infty \frac{2}{\pi} \tan^{-1}(ke_{py}^{[i]})) - \rho\bar{\chi}^{[i]}\text{sgn}\,\bar{\chi}^{[i]}$$

$$= -\rho\bar{\chi}^{[i]}\text{sgn}\,\bar{\chi}^{[i]} - e_{py}^{[i]} V_g^{[i]} \sin(\chi_\infty \frac{2}{\pi} \tan^{-1}(ke_{py}^{[i]}))$$

$$+ e_{py}^{[i]} V_g^{[i]} \left[\sin(\bar{\chi}^{[i]} - \underbrace{\chi_\infty \frac{2}{\pi} \tan^{-1}(ke_{py}^{[i]})}_{=-\chi_{de}^{[i]}}) - \sin\chi_{de}^{[i]} \right]$$

$$\leq -\rho\bar{\chi}^{[i]}\text{sgn}\,\bar{\chi}^{[i]} + e_{py}^{[i]} V_g^{[i]} \sin\chi_{de}^{[i]}$$

$$+ V_g^{[i]} |e_{py}^{[i]}| |\sin(\bar{\chi}^{[i]} + \chi_{de}^{[i]}) - \sin\chi_{de}^{[i]}|$$

It notes the following:

$$|\sin(\bar{\chi}^{[i]} + \chi_{de}^{[i]}) - \sin\chi_{de}^{[i]}|$$

$$= |\sin(\bar{\chi}^{[i]} \cos\chi_{de}^{[i]}) + \cos(\bar{\chi}^{[i]} \sin\chi_{de}^{[i]}) - \sin\chi_{de}^{[i]}|$$

$$= |\sin\chi_{de}^{[i]}(\cos(\bar{\chi}^{[i]} - 1) + \sin(\bar{\chi}^{[i]} \cos\chi_{de}^{[i]})|$$

$$\leq |\cos(\bar{\chi}^{[i]} - 1)| + |\sin\bar{\chi}^{[i]}|$$

$$\leq 2|\bar{\chi}^{[i]}|$$

and given $|\bar{\chi}^{[i]}| = \bar{\chi}^{[i]}\text{sgn}\,\bar{\chi}^{[i]}$, one obtains the following:

$$\dot{V}^{[i]} \leq -\rho|\bar{\chi}^{[i]}| + e_{py}^{[i]} V_g^{[i]} \sin\chi_{de}^{[i]} + 2V_g^{[i]} |e_{py}^{[i]}| |\bar{\chi}^{[i]}|$$

Let

$$\phi(e_{py}^{[i]}) = e_{py}^{[i]} \sin\left(\frac{2\chi_\infty}{\pi} \tan^{-1}(ke_{py}^{[i]}) \right)$$

and note the following:

$$\left| \frac{\partial\phi}{\partial e_{py}^{[i]}} \right| = \left| \sin\left(\frac{2\chi_\infty}{\pi} \tan^{-1}(ke_{py}^{[i]}) \right) \right.$$

$$\left. + e_{py}^{[i]} \cos\left(\frac{2\chi_\infty}{\pi} \tan^{-1}(ke_{py}^{[i]}) \right) \frac{2\chi_\infty}{\pi} \frac{k}{1 + (ke_{py}^{[i]})^2} \right|$$

$$\leq \left| \frac{2\chi_\infty}{\pi} \tan^{-1}(ke_{py}^{[i]}) \right| + \left| \frac{2\chi_\infty}{\pi} \frac{k}{1 + (ke_{py}^{[i]})^2} \right|$$

$$\leq 2k|e_{py}^{[i]}| \frac{2\chi_\infty}{\pi}$$

Using the fact that if f and g are continuous functions such that $f(0) = g(0)$ and $|\dot{f}(x)| \leq |\dot{g}(x)|$, then $|f(x)| \leq |g(x)|$, one has the following:

$$\dot{V}^{[i]} \leq -\rho|\bar{\chi}^{[i]}|^2 - 2kV_g^{[i]} |e_{py}^{[i]}|^2 \frac{2\chi_\infty}{\pi} + 2V_g^{[i]} |e_{py}^{[i]}| |\bar{\chi}^{[i]}| \tag{12}$$

$$= -V_g^{[i]} \begin{bmatrix} |\bar{\chi}^{[i]}| & |e_{py}^{[i]}| \end{bmatrix} \begin{bmatrix} \frac{\rho}{V_g^{[i]}} & -1 \\ -1 & \frac{4\chi_\infty}{\pi}k \end{bmatrix} \begin{bmatrix} |\bar{\chi}^{[i]}| \\ |e_{py}^{[i]}| \end{bmatrix} \tag{13}$$

As a result, (12) is negative if the following holds true:

$$\frac{\rho}{V_g^{[i]}} \frac{4\chi_\infty k}{\pi} - 1 > 0.$$

□

3.3. A Longitudinal Guidance

Lemma 3 simply ensures that the UAVs, $p^{[i]}$, follow the predefined path, $\mathcal{P}_{line}^{[i]}, i \in \mathcal{N}$, as section 3.2 demonstrates. This implies that the lateral distance satisfies $\lim_{t\to\infty} \|e_{py}^{[i]}\| \to 0$. The following result gives a suggested method for coordinating UAVs, and follows a desired course angle. The formation path-following under delays is handled by Algorithm 1.

Algorithm 1 A Guidance of Straight-Line Formation

1: **procedure** DETERMINE A STRAIGHT LINE
2:　　Set up a desired course χ_d, a leader's root r^l, and relative positions $\Gamma^{[i]}$
3:　　Determine the path's root for UAV$^{[i]}$

$$r^{[i]} \leftarrow r^l + \begin{bmatrix} \cos(\chi_d) & \sin(\chi_d) \\ -\sin(\chi_d) & \cos(\chi_d) \end{bmatrix} \Gamma^{[i]}$$

4:　　Determine the UAV$^{[i]}$'s straight line

$$\{\mathcal{P}_{line}^{[i]} : p^{[i]} \leftarrow r^{[i]} + \lambda[\cos(\chi_d) \; \sin(\chi_d)] \in \mathbb{R}^2\}$$

5: **end procedure**
1: **procedure** DETERMINE A COURSE ANGLE
2:　　Set up a UAV's root $r^{[i]}$, a UAV's position $p^{[i]}$, guidance parameters k, k_{sl}, and desired and current course $\chi_d, \chi^{[i]}$
3:　　Determine a distance

$$e_{py}^{[i]} \leftarrow [-\sin\chi_d, \cos\chi_d](p^{[i]} - r^{[i]})$$

4:　　Determine commanded course angle

$$\chi_c^{[i]} \leftarrow \chi^{[i]} - \frac{k_{sl}}{1 + (ke_{py}^{[i]})^2} \sin(\chi^{[i]}) - \frac{\rho}{\alpha} \mathrm{sgn}\, \bar{\chi}^{[i]}$$

5: **end procedure**
1: **procedure** DETERMINE A DESIRED AIRSPEED
2:　　Determine a projection of $p^{[i]} - r^{[i]}$

$$e_{px}^{[i]} \leftarrow [\cos\chi_d, \sin\chi_d](p^{[i]} - r^{[i]})$$

3:　　Determine a UAV$^{[i]}$'s desired airspeed

$$V_{ad}^{[i]} \leftarrow V_d + \kappa \sum_{i=1}^{N} a_{ij} \left[e_{px}^{[i]}(t-\tau) - e_{px}^{[j]}(t-\tau) \right] \tag{14}$$

4: **end procedure**

Next, our key strategy to address the formation guidance problem is to maintain the UAVs' longitudinal distance along the planned path. It allows a UAV swarm to reach a V-shaped formation. To do this, UAVs $V_{ad}^{[i]}$ alter their command airspeed in proportion to

their longitudinal distance. UAV$^{[i]}$'s airspeed, for instance, will be set to a maximum value if the UAV's position is too far from the average UAV's position and otherwise. Thus, each UAV's desired airspeed is determined utilizing Algorithm 1, as given in (14), where the longitudinal distance between the UAV and the desired path is represented by $e_{px}^{[i]}$ in (5). As a result, the theorem gives our main results.

Theorem 1. *Assuming that $\mathcal{P}_{line}^{[i]}$ and $\chi_c^{[i]}$ can be determined to satisfy (8) and Lemma 3, UAV swarms reach a V-shaped formation if the airspeed $V_{ad}^{[i]}$ for UAV$^{[i]}$ is provided by Algorithm 1, where $\kappa > 0$, $\tau = \left[0, \frac{\pi}{2\kappa\lambda_N}\right)$, and $\lambda_N = max\{\|\lambda_i(\mathcal{L})\|\}_{i=2}^N$, which means the following:*

$$\lim_{t\to\infty}\left[(p^{[i]} - r^{[i]}) - (p^{[j]} - r^{[j]})\right] \to 0 \tag{15}$$

Proof. The longitudinal dynamics of UAV$^{[i]}$, $i \in \mathcal{N}$, are given as follows:

$$\dot{e}_{px}^{[i]} = V_{ad}^{[i]}, i = 1, 2, \cdots, N \tag{16}$$

and using the formation control law in (14), one obtains the following:

$$\dot{e}_{px}^{[i]} = V_d + \kappa \sum_{i=1}^N a_{ij}\left[e_{px}^{[i]}(t - \tau) - e_{px}^{[j]}(t - \tau)\right] \tag{17}$$

and using the Laplacian matrix $\mathcal{L} = [l_{ij}] \in \mathbb{R}^{N\times N}$ in section 3.1, one has the following:

$$\dot{\mathbf{e}}_{px} = \mathbf{1}V_d - \kappa\mathcal{L}\mathbf{e}_{px}(t - \tau)$$

Next, the longitudinal distance $e_{px}^{[i]}$ in (17) represents the coordination states of the UAVs. Let the following:

$$z^{[i]} = e_{px}^{[i]} - \sum_{j \in N_i} f_j e_{px}^{[j]}$$

be the coordination error between UAVs, where f_i is the i component of the left eigenvector of the Laplacian matrix. Because the graph is connected to an undirected graph, $\mathbf{f} = \frac{1}{N}\mathbf{1}$, where $\mathbf{1} = [1]_{N\times 1}$. In this case, z_i is a disagreement vector between the coordination state $e_{px}^{[j]}$ and the average of all coordination states. Additionally, let $\mathbf{z} = [z^{[1]}, z^{[2]}, \cdots, z^{[N]}]^T \in \mathbb{R}^N$, which is re-expressed as follows:

$$\mathbf{z} = (\mathbf{I} - \mathbf{1}\mathbf{f}^T)\mathbf{e}_{px}; \mathbf{W} = \mathbf{I} - \mathbf{1}\mathbf{f}^T,$$

where $\mathbf{W}$ satisfies the following properties:

$$\mathbf{W}\mathbf{1} = 0; \mathbf{W}\mathcal{L} = \mathcal{L}\mathbf{W} \tag{18}$$

With the above definition, it is clear that the UAV swarms reach formation if all coordination UAVs' states are synchronized, that is,

$$\lim_{t\to\infty}(\mathbf{e}_{px}^{[i]} - \mathbf{e}_{px}^{[j]}) \to 0$$

$$\Leftrightarrow \lim_{t\to\infty}[\cos\chi_d, \sin\chi_d]\left[(p^{[i]} - r^{[i]}) - (p^{[j]} - r^{[j]})\right] \to 0$$

$$\Leftrightarrow \lim_{t\to\infty}\left[(p^{[i]} - r^{[i]}) - (p^{[j]} - r^{[j]})\right] \to 0$$

if and only if $\mathbf{z} = 0$. As a result, the dynamics of $\mathbf{z}$ are represented as follows:

$$
\begin{aligned}
\dot{\mathbf{z}} &= \mathbf{W}\dot{\mathbf{e}}_{px} \\
&= \mathbf{W}(\mathbf{1}V_d - \kappa\mathcal{L}\mathbf{e}_{px}(t-\tau))
\end{aligned}
\tag{19}
$$

In the following, $\mathcal{G}$ is a fixed and connected undirected graph with the following linear delay differential system:

$$
\dot{\mathbf{z}} \overset{(18)}{=} -\kappa\mathcal{L}\mathbf{z}(t-\tau)
\tag{20}
$$

where eigenvalues of $\mathcal{L}$ satisfy $\{\kappa\lambda_i\}_{i=2}^{N} \in \mathbb{R}_{>0}$. Then, by employing the straightforward application of Lemma 1, one has the following:

$$
\left\| \tan^{-1}\left[\frac{Re(\lambda_i)}{Im(\lambda_i)} \right] \right\| = \frac{\pi}{2}
$$

and $max\{k\|\lambda_i\|\}_{i=2}^{N} = k\lambda_N$. Therefore, the delay system (20) is asymptotically stable if and only if the following condition holds:

$$
0 \leq \tau < \frac{\pi}{2\kappa\lambda_N}
\tag{21}
$$

Let $\lambda_i(\mathcal{L})$ stand for the eigenvalue of $\mathcal{L}$ and $v_{min} = min\{Re(\lambda_i(\mathcal{L}))\}$. From Lemma 2, the eigenvalue $v_{min} > 0$. Then, we know that for any $Y \in (0, v_{min})$, there is a positive-definite matrix $Y \in \mathbb{R}^{N \times N}$, such that the following holds:

$$
\mathcal{L}^T Y + Y\mathcal{L} - 2YY > 0
\tag{22}
$$

In other words, since time delay τ satisfies (21), the Lyapunov function is considered as follows:

$$
V(t) = \mathbf{z}^T Y \mathbf{z}
$$

where Y is given in (22), and then the Lyapunov function satisfies the following condition:

$$
\begin{aligned}
\dot{V}(t) &= -z^T(\mathcal{L}^T Y + Y\mathcal{L})z \\
&\overset{(22)}{\leq} -\kappa Y \mathbf{z}^T Y \mathbf{z} \\
&= -kV(t), \quad \text{where } k = \kappa Y > 0
\end{aligned}
$$

$\square$

4. Loitering Path Formation under Communication Delay

The loitering formation algorithm generates vector fields in a way similar to the formation's straight line. Specifically, the loitering formation problem given in Section 2.2 consists of three components: The specification of a circular line for UAV swarms ensures that all intended UAV trajectories are concentric and equidistant. The UAV is then directed laterally to follow the planned trajectory. Finally, a longitudinal guidance mechanism is presented to enable the formation of UAV swarms with communication delays.

4.1. Define Circular Line

The concentric and equidistant circular pathways $\mathcal{P}_{cir}^{[i]}$, $i = 1, 2, \cdots, N$ for UAVs are one of their defined paths' goals. A circle-line definition for $\text{UAV}^{[i]}$ is formed in part by the suggested formation, the radius of the circular $R^{[i]}$, the desired direction λ of UAV swarms, and the S-point p_w.

First, each UAV's circular line radius is calculated using (23), as follows:

$$R^{[i]} = R^{[l]} + \Gamma^{[i]} \tag{23}$$

where each S-point p_w represents a waypoint of UAV swarms (*specified by an operator*), $\Gamma^{[i]}$ indicates the relative distance among UAV$^{[i]}$ in the network, and $R^{[l]}$ is the current radius of a specified UAV, termed a leader. Additionally, the vector $\boldsymbol{\Gamma} = [\Gamma^{[1]}, \cdots, \Gamma^{[N]}]^T \in \mathbb{R}^2$ defines the shape of a formation.

As a result, the defined paths $\mathcal{P}_{cir}^{[i]}$, $i = 1, 2, \cdots, N$ for UAVs are given as follows:

$$\{\mathcal{P}_{cir}^{[i]} : p^{[i]} \leftarrow p_w + \lambda R^{[i]}[cos(\varrho) \; sin(\varrho)] \in \mathbb{R}^2\} \tag{24}$$

4.2. A Lateral Guidance

We design a process where UAV$^{[i]}$ follows the intended path $\mathcal{P}_{cir}^{[i]}$ in (24), as stated in Section 4.1. Our suggested algorithm, which makes use of a vector field technique, ensures that UAV$^{[i]}$ will move across a circular path $\mathcal{P}_{cir}^{[i]}$. A reference course for guiding UAV$^{[i]}$ along the path is provided as follows:

$$\chi_d^{[i]} = \eta^{[i]} + \lambda \left[\frac{\pi}{2} + \tan^{-1}\left(k\frac{\rho^{[i]} - R^{[i]}}{R^{[i]}} \right) \right] \tag{25}$$

where the distance of S-point and UAV$^{[i]}$ is as follows:

$$\rho^{[i]} = \|p^{[i]} - p_w\|, \tag{26}$$

an angular position of UAV$^{[i]}$ to S-point is as follows:

$$\eta^{[i]} = \tan^{-1}(p_n^{[i]} - p_{nw}, p_e^{[i]} - p_{ew}), \tag{27}$$

and there is a positive parameter k.

To guarantee $\chi^{[i]} \to \chi_d^{[i]}$ and $\rho^{[i]} \to R^{[i]}$ as $t \to 0$, Equation (28) gives a course angle, where $k_{sc} = \lambda \|V_g\| \frac{\vartheta}{\alpha}$. Moreover, control aggressiveness is governed by ϑ, α, which also mitigate any potential chattering in a control action.

$$\chi_c^{[i]} = \chi^{[i]} + \frac{k_{sc}}{1 + k\|\rho^{[i]} - R^{[i]}\|^2} \cos(\chi^{[i]} - \eta^{[i]}) \tag{28}$$

$$+ \frac{\|V_g^{[i]}\|}{\alpha\rho^{[i]}} \sin(\chi^{[i]} - \eta^{[i]}) + \frac{\vartheta}{\alpha}\text{sgn}\,(\chi^{[i]} - \chi_d^{[i]})$$

Let $\bar{\chi}^{[i]} = \chi^{[i]} - \chi_d^{[i]}$ and $\bar{\rho}^{[i]} = \rho^{[i]} - R^{[i]}$; their dynamics can be described by using (2), (6), and (25), as follows:

$$\dot{\bar{\rho}}^{[i]} = V_g^{[i]} \sin(\chi^{[i]} - \eta^{[i]})$$

$$\dot{\bar{\chi}}^{[i]} = \alpha(\chi_c^{[i]} - \chi^{[i]}) + \beta^{[i]} \cos(\chi^{[i]} - \eta^{[i]}) + \frac{1}{\alpha\rho^{[i]}}\dot{\bar{\rho}}^{[i]} \tag{29}$$

where $\beta^{[i]} = \frac{k_{sc}}{1 + k\|\rho^{[i]} - R^{[i]}\|^2}$ is defined for brevity.

As a result, one has the following lemma:

Lemma 4. *The system* (29) *with* $\chi_c^{[i]}$ *is given in* (28), *which is asymptotically stable, which means the following:*

$$\lim_{t \to \infty} \left[\rho^{[i]}(t) - R^{[i]} \right] \to 0,$$

$$\lim_{t \to \infty} \bar{\chi}^{[i]}(t) \to 0$$

if $\frac{2k\vartheta}{\alpha V_g^{[i]} R^{[i]}} > 1$, *where* $\vartheta > 0$.

Proof. We consider the following Lyapunov function:

$$V^{[i]} = \frac{1}{2} \left(\bar{\rho}^{[i]} \right)^2 + \frac{1}{2} \left(\bar{\chi}^{[i]} \right)^2$$

The rest of the proof is similar to Lemma 3. □

4.3. A Longitudinal Guidance

The airspeed of the UAVs $V_{ad}^{[i]}$ is modified in the following to solve the formation guidance issue with regard to the offset angle between the UAV and the north. Thus, Algorithm 2 computes the required airspeed for each UAV, as follows:

Algorithm 2 A Guidance Algorithm of Loitering Formation

1: **procedure** DETERMINE CIRCULAR LINE
2:     Set up an S-point p_w, a leader's radius $R^{[l]}$, a desired distance of UAVs $\Gamma^{[i]}$, a direction λ, and $\varrho \in [0, 2\pi]$
3:     Determine a circular's radius of UAV$^{[i]}$

$$R^{[i]} \leftarrow R^{[l]} + \Gamma^{[i]}$$

4:     Determine the circular's path of UAV$^{[i]}$

$$\{ \mathcal{P}_{cir}^{[i]} : p^{[i]} \leftarrow p_w + \lambda R^{[i]} [\cos(\varrho) \ \sin(\varrho)] \in \mathbb{R}^2 \}$$

5: **end procedure**
1: **procedure** DETERMINE A COMMANDED COURSE
2:     Set up an S-point of UAV swarm p_w, a loiter direction λ, a radius $R^{[i]}$, $p^{[i]}$, course angle $\chi^{[i]}$, and gain k
3:     Determine the distance between an S-point and UAV

$$\rho^{[i]} = \| p^{[i]} - p_w \|$$

4:     Determine the angular position in relation to the waypoint

$$\eta^{[i]} = \text{atan2}(p_n^{[i]} - p_{nw}, p_e^{[i]} - p_{ew})$$

5:     Determine the specified course angle

$$\chi_c^{[i]} = \chi^{[i]} + \frac{k_{sc}}{1 + k \| \rho^{[i]} - R^{[i]} \|^2} \cos(\chi^{[i]} - \eta^{[i]})$$

$$+ \frac{\| V_g^{[i]} \|}{\alpha \rho^{[i]}} \sin(\chi^{[i]} - \eta^{[i]}) + \frac{\vartheta}{\epsilon} \text{sgn} \left(\chi^{[i]} - \chi_d^{[i]} \right)$$

6: **end procedure**

Algorithm 2 *Cont.*

1: **procedure** DETERMINE A COOPERATIVE AIRSPEED

2:     Set up an S-point p_w, UAVs' position $p^{[i]}$, leader's radius $R^{[l]}$, and offset of angular position $\eta_o^{[i]}$

3:     Determine an error of angle between UAV$^{[i]}$ and $\eta_o^{[i]}$

$$\bar{\eta}^{[i]} = \eta^{[i]} - \eta_o^{[i]} \tag{30}$$

4:     Determine a distance between S-point p_w and UAV$^{[i]}$ position

$$\rho^{[i]} \leftarrow \| p^{[i]} - p_w \| \tag{31}$$

5:     Determine a cooperative airspeed of UAV$^{[i]}$

$$V_{ad}^{[i]} \leftarrow \frac{\rho^{[i]} V_d}{R^{[l]}} + \rho^{[i]} \kappa \sum_{j=1}^{N} a_{ij} \left[\bar{\eta}^{[i]}(t - \tau) - \bar{\eta}^{[j]}(t - \tau) \right] \tag{32}$$

6: **end procedure**

Our results give the theorem as follows:

Theorem 2. *Assuming that $\mathcal{P}_{cir}^{[i]}$ and $\chi_c^{[i]}$ can be chosen to fulfill (24) and Lemma 4, UAV swarms reach loitering formation if Algorithm 2 determines the demanded airspeed $V_{ad}^{[i]}$ for UAV$^{[i]}$, where $\kappa > 0, \tau = \left[0, \frac{\pi}{2\bar{\kappa}\lambda_N}\right)$, and $\lambda_N = max\{\|\lambda_i(\mathcal{L})\|\}_{i=2}^N$, which means the following:*

$$\lim_{t \to \infty} \left[(\eta^{[i]} - \eta_o^{[i]}) - (\eta^{[j]} - \eta_o^{[j]}) \right] \to 0, i \in \mathcal{N} \tag{33}$$

Proof. Before giving the proof of Theorem 2, the dynamics of the longitudinal motion of UAV$^{[i]}, i \in \mathcal{N}$ is rewritten as follows:

$$\dot{\eta}^{[i]} = \frac{V_{ad}^{[i]}}{R^{[i]}}, i = 1, 2, \cdots, N \tag{34}$$

Using the formation control law in (32), one obtains the following:

$$\dot{\eta}^{[i]} = \frac{V_d}{R^{[l]}} + \kappa \sum_{j=1}^{N} a_{ij} \left[\bar{\eta}^{[i]}(t - \tau) - \bar{\eta}^{[j]}(t - \tau) \right] \tag{35}$$

Using the Laplacian matrix $\mathcal{L}$, which describes the communication among UAVs, in Section 3.1, one has the following:

$$\dot{\bar{\eta}} = \mathbf{1}\bar{V}_d - \kappa \mathcal{L}\bar{\mathbf{j}}(t - \tau) \tag{36}$$

where $\bar{V}_d = \frac{V_d}{R^{[l]}}$. The next step is the same as in the proof of Theorem 1. □

5. UAV Swarm Benchmark

We first examine the UAV's autopilot system's architecture before providing a benchmark for UAV swarms. As shown in Figure 4, an autopilot (AP) typically comprises the throttle δ_t, elevator δ_e, and aileron δ_a.
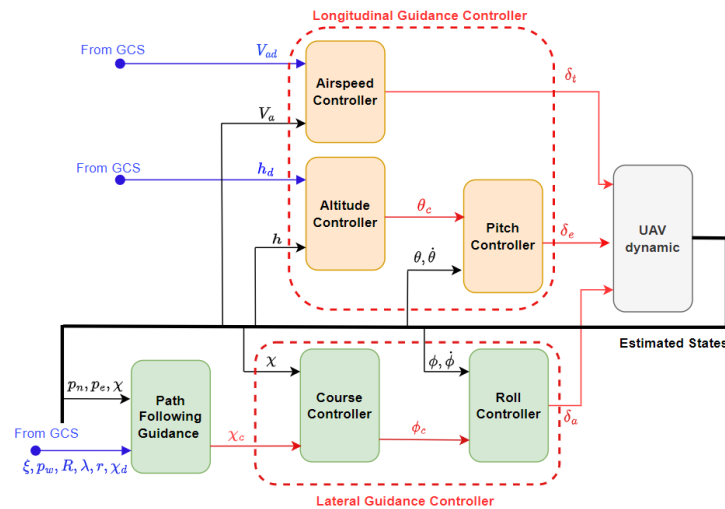
Figure 4. Fixed-wing UAV guidance and control structures. GCS data are shown in blue code, and AP data on the UAVs are shown in red code. The control loops (blocks) are shown in light orange code with respect to longitudinal guidance and in light green code with respect to lateral guidance.

The fixed-wing UAV's inertial position (p_n, p_e, h) and attitude (ϕ, θ, χ) are preserved using the AP algorithms. Specifically, the majority of important flying maneuvers are developed using AP systems considering decoupled dynamics. Control algorithms are thought to be able to minimize undesired effects, or disruptions. We consider that the longitudinal dynamics are decoupled from the lateral dynamics, as illustrated in Figure 4. This leads to the simple construction of the autopilot systems and enables us to use commonly used methods such as consecutive loop closure, as described in [27].

Furthermore, by analyzing data from the on-board sensor and the ground control station (GCS), the actuators' intended values are calculated by the AP module. The data packet sent from GCS as shown in Figure 4 has the flight mode change command; desired altitude h_d, desired airspeed V_{ad}, tracking mode ξ, circle data (*S-point* $p_w \in \mathbb{R}^2$, *radius R*, *loiter direction* λ), and tracking straight-line path data (*root point* $r \in \mathbb{R}^2$ *and desired course* χ_d) are typically included.

Matlab Simulink has been utilized to implement the dynamics of fixed-wing UAVs and wind. The kinematics and dynamics of fixed-wing UAVs are described in [27], while wind is modeled as a combination of dynamic and constant components, as demonstrated in [5].

$$V_{wg} = \begin{cases} 0 & x < 0 \\ V_{mg}\left(1 - \cos(\frac{\pi x}{d_{mg}})\right) & 0 \leq x \leq d_{mg} \\ V_{mg} & x > d_{mg} \end{cases}$$

Note here that Algorithms 1 and 2 are implemented on the UAV and GCS. In particular, GCS computes the desired path $\mathcal{P}_{line}^{[i]}$, $\mathcal{P}_{cir}^{[i]}$, $i \in \mathcal{N}$, and desired airspeed $V_{ad}^{[i]}$ for UAV$^{[i]}$, and AP calculates the course angle $\chi_c^{[i]}$. Furthermore, given some limitations on $\phi^{[i]}$ (rad) and $V_a^{[i]}(\frac{m}{s})$, aerodynamic coefficients for fixed-wing UAVs are reported in [27] as follows:
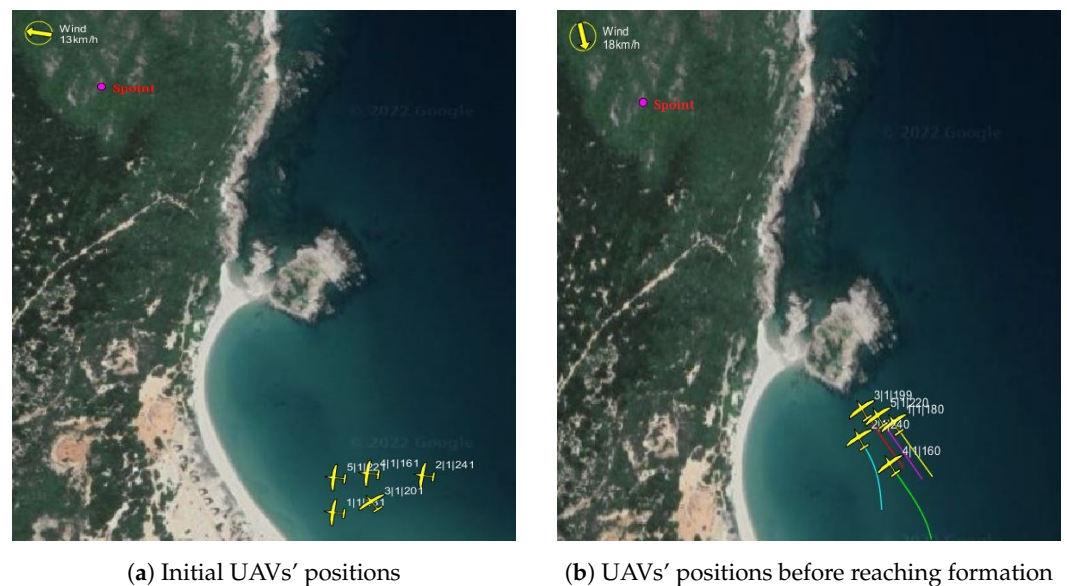
$$|\phi^{[i]}| \leq \frac{\pi}{4}; \ 25 \leq V_a^{[i]} \leq 33 \tag{37}$$

and UAV swarms are initiated with certain parameters, as shown in Table 1. After that, the aforementioned initial conditions and limitations are implemented in Algorithms 1 and 2.

Table 1. Initial condition of 5 UAVs, $i = 1, \cdots, 5$.

UAVs' Initial	Values
Position's east and north (m)	$|p_n^{[i]}(0)|, |p_e^{[i]}(0)| \leq 400$
Altitude (m)	$h^{[i]}(0) \in [450, 550]$
Airspeed (m/s)	$V_a^{[i]}(0) \in [22, 33]$
Angle of roll and pitch (rad)	$|\phi^{[i]}(0)|, |\phi^{[i]}(0)| \leq \frac{\pi}{4}$
Angle of yaw (rad)	$|\psi^{[i]}(0)| \leq \pi$
Rate's angular (rad/s)	$\|\Omega^{[i]}(0)\| \leq 0.05$

The results of simulations are depicted in Figures 5a,b and 6 regarding straight-line formation and Figure 7a,b corresponding to loitering formation, where the direction and value of wind are displayed on the left corner of the figure. It is evident that UAVs generate the planned V-shape. The violet point in the figure, called S-point, plays a role as a waypoint that UAV swarm will move toward. Please see the link video at https://youtu.be/Y4YOXMCHfOw (accessed on 17 October 2022) for more detail.

(**a**) Initial UAVs' positions

(**b**) UAVs' positions before reaching formation

**Figure 5.** Evolution of UAVs' positions before reaching formation.

**Figure 6.** UAV swarm reaches a V-shaped formation.

(**a**) UAVs' positions before reaching loitering　　(**b**) UAV swarm reaching loitering formation

Figure 7. Evolution of UAVs' positions.

This is further demonstrated by consensus on a course angle in an interval time $[0 \ 130(s)]$ and airspeed as depicted in Figures 8 and 9, respectively. In the meantime, Algorithm 2 is implemented for a circular-path formation.
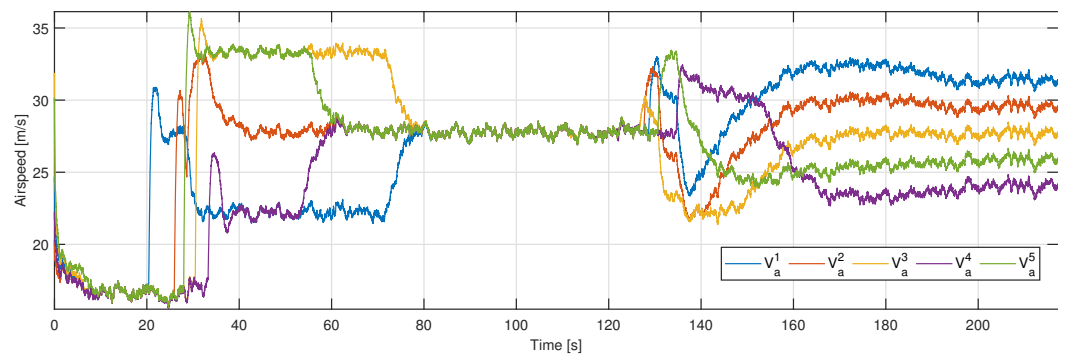

Figure 8. Airspeed of UAVs.
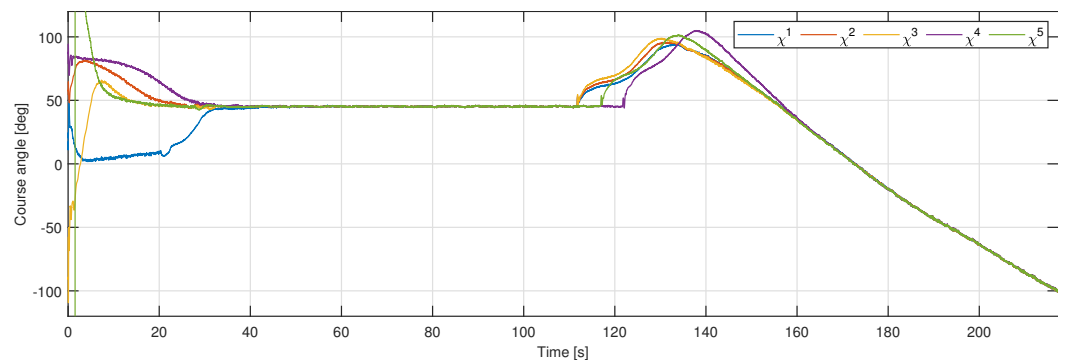
Figure 9. Course angles of UAVs

The result simulation splits into two stages: in the interval time $[0 \ 130](s)$, five UAVs reach the straight-line formation, and they achieve the loitering formation in the rest time. Considering the first state, it is clear that UAVs will maneuver the same direction and track a parallel straight-line path, i.e., $\chi^{[1]} = \chi^{[2]} = \chi^{[3]} = \chi^{[4]} = \chi^{[5]}$ (see Figure 6). In the meantime, UAVs reach consensus with the airspeed $V_a^{[1]} = V_a^{[2]} = V_a^{[3]} = V_a^{[4]} = V_a^{[5]}$ (see Figure 5), which helps achieve and maintain the V-shaped formation. It is similar in the case of the loitering formation of the second stage, where UAVs will fly in the same direction $\chi^{[i]}$ and with a different airspeed $V_a^{[i]}$ to reach and maintain the V-shaped formation.

6. Hardware-in-the Loop (HIL) Test

As shown in Figure 10a, we built an efficient and reliable platform for the HIL testing of UAV swarm, which consists of three primary components: fixed-wing UAV, GDT (Ground Data Terminal) system, and GCS systems, also known as C4I (Command, Control, Communication, Computer, and Intelligence).
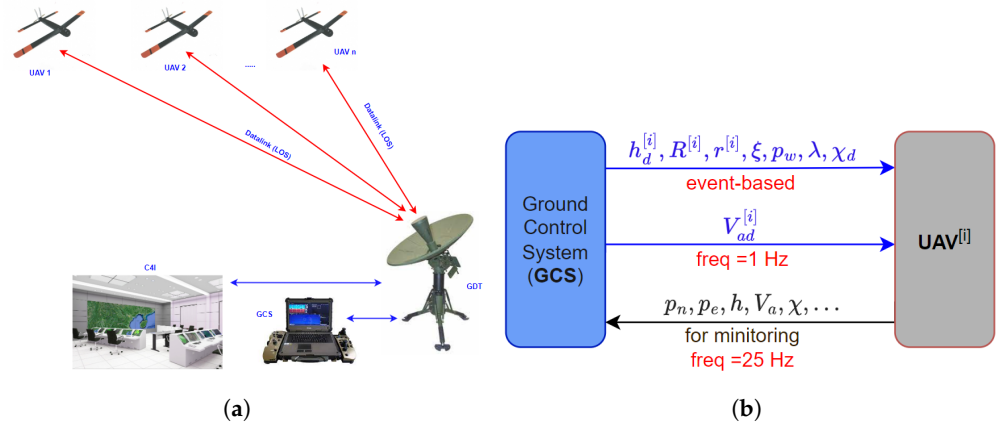

Figure 10. Interaction between GCS and UAVs: (**a**) illustrative interaction among GCS and UAVs; (**b**) exchanged information between GCS and UAVs.

The parts' primary goal in our expansion is as follows:

- UAV Swarms: The five fixed-wing UAV swarms' platform. Each UAV has AutoPilot-AP systems, which are implemented in C++. These systems compute the lateral and longitudinal controllers for inertial position $(p_n^{[i]}, p_e^{[i]}, h^{[i]})$ and attitude $(\phi^{[i]}, \theta^{[i]}, \chi^{[i]})$, respectively.
- GCS: C$^{\#}$ is used to write the ground control system (GCS), which gives the tracker's (pilot) the ability to modify waypoints in order to monitor and regulate UAV behavior. The tracker is able to observe the experiments' progress because UAV telemetry is shown in real time in the GCS. Real-time maps are downloaded from the Internet using a 4G modem. Video capture modules, telemetry modems, and 4G modems may all send data to the GCS computer via USB ports. In practice, the GCS is limited to a 5-kilometer radius due to the telemetry system's communication range with the UAV.
- Datalink: The ground data terminal (GDT) allows full-duplex communication by means of a radio link established between the UAV and the GCS computer. An air data terminal (ADT) receives telemetry data from the GCS when an autonomous aircraft is in flight, and it forwards these data to the flight control system (FCS).

Specifically, the GCS facilitates the information exchanged between UAVs in the network, as seen in Figure 10b. This implies that a UAV transmits its data, which include its current location $p^i = [p_n^{[i]}, p_n^{[i]}]$, course angle $\chi^{[i]}$, airspeed $V_a^{[i]}$, and attitude $h^{[i]}$, to the GCS at a predetermined frequency of 25 Hz. Meanwhile, the GCS computes the tracking path information and generates the required airspeed for UAV$^{[i]}$ based on Algorithms 1 and 2 using the data received from UAV$^{[i]}$ and other UAVs. Subsequently, the UAV will receive these data over a communication network. The tracking path includes the following: path direction λ, root $r^{[i]}$, tracking mode ξ, waypoint $p_w^{[i]}$, radius $R^{[i]}$, attitude $h_d^{[i]}$, and designed course $\chi_d^{[i]}$. As shown in Figure 10b, the required airspeed $V_a^{[i]}$ communicates with the frequency at 1 Hz, and the communication from the GCS to the UAV is event-based. In conclusion, the GCS has to address two problems in order to enable swarm formation path-following: (i) calculating each UAV's expected airspeed and sending it regularly and (ii) determining the path's tracking for each UAV and sending it, which is based on an event whenever the path's parameters change.

Furthermore, to calculate a commanded course angle $\chi_c^{[i]}$ for the path's tracking, the AP system utilizes Algorithm 1. It is founded from data that were obtained from the GCS. The experiment was conducted as shown in Figure 11, and the GCS is also shown there (see Figure 12). To discover more, see the video at https://youtu.be/Ot5-7JfdjjA (accessed on 23 February 2022). It is evident that five fixed-wing UAVs are able to create loitering and V-shaped formations.
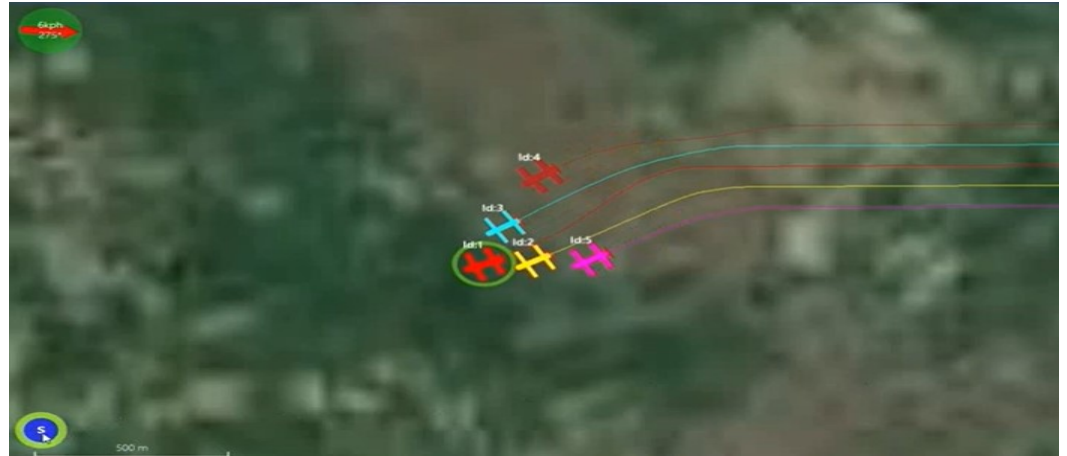
Figure 11. Loitering formation of UAV swarm.
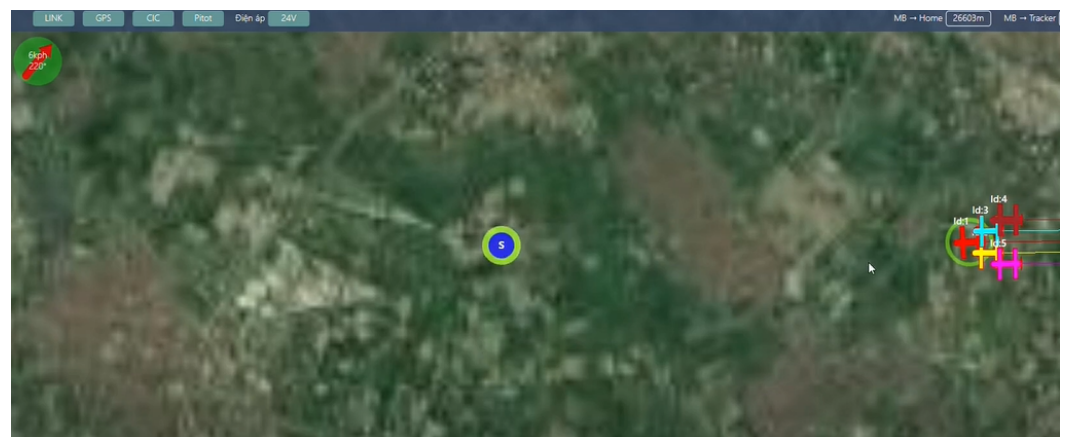
Figure 12. V-shaped formation of UAV swarm.

7. Conclusions

We have presented cooperative path-following guidance with communication delays in this research. When there is wind disturbance, a vector field is utilized to calculate a course angle. This allows all UAVs to follow a predetermined path. A longitudinal motion-related airspeed consensus algorithm under delay communication has been also developed. In addition, we have provided an information exchange between a GCS and UAVs using different frequencies. A rigorous platform flying HIL test and a benchmark UAV swarm have been generated to validate our theoretical results. We have left a few intriguing open-ended topics for our further research, such as how to handle angle-constrained formation control problems within a Leader-First Follower of fixed-wing UAVs' sensing framework.

Author Contributions: Conceptualization, T.D.N. and T.V.P.; methodology, T.V.P.; software, T.V.P. and T.D.N.; validation, T.V.P. and T.D.N.; formal analysis, T.V.P.; investigation, T.V.P.; resources, T.D.N.; data curation, T.D.N. and T.V.P.; writing—original draft preparation, T.V.P.; writing—review and editing, T.V.P.; visualization, T.D.N. and T.V.P. All authors have read and agreed to the published version of the manuscript.

Conflicts of Interest: The authors declare no conflicts of interest.

References

1. Vu, D.V.; Pham, T.V.; Nguyen, D.T. A path-following guidance algorithm for fixed-wing UAV swarms on a decentralized network. In Proceedings of the 2022 International Conference on Advanced Technologies for Communications (ATC), Ha Noi, Vietnam, 20–22 October 2022; pp. 286–291.
2. Chen, H.; Wang, X.; Shen, L.; Yu, Y. Coordinated path following control of fixed-wing unmanned aerial vehicles in wind. *ISA Trans.* **2022**, *122*, 260–270. [CrossRef] [PubMed]
3. Zeng, L.; Liao, X.; Ma, Z.; Xiong, B.; Jiang, H.; Chen, Z. Three-Dimensional UAV-to-UAV Channels: Modeling, Simulation, and Capacity Analysis. *IEEE Internet Things J.* **2024**, *11*, 10054–10068. [CrossRef]
4. Lan, Y.; Yan, G.; Lin, Z. Synthesis of Distributed Control of Coordinated Path Following Based on Hybrid Approach. *IEEE Trans. Autom. Control* **2011**, *56*, 1170–1175. [CrossRef]
5. Pengzhi, T.; Chao, H.; Rhudy, M.; Gross, J.; Wu, H. Wind sensing and estimation using small fixed-wing unmanned aerial vehicles: A survey. *J. Aerosp. Inf. Syst.* **2021**, *18*, 132–143.
6. Chen, H.; Wang, X.; Shen, L.; Cong, Y. Formation flight of fixed-wing UAV swarms: A group-based hierarchical approach. *Chin. J. Aeronaut.* **2021**, *34*, 504–515. [CrossRef]
7. Roldão, V.; Cunha, R.; Cabecinhas, D.; Silvestre, C.; Oliveira, P. A leader-following trajectory generator with application to quadrotor formation flight. *Robot. Auton. Syst.* **2014**, *62*, 1597–1609. [CrossRef]
8. Kushleyev, A.; Mellinger, D.; Powers, C.; Kumar, V. Towards a swarm of agile micro quadrotors. *Auton. Robot.* **2013**, *35*, 287–300. [CrossRef]
9. Cichella, V.; Choe, R.; Mehdi, S.B.; Xargay, E.; Hovakimyan, N.; Dobrokhodov, V.; Kaminer, I.; Pascoal, A.M.; Aguiar, A.P. Safe coordinated maneuvering of teams of multirotor unmanned aerial vehicles: A cooperative control framework for multivehicle, time-critical missions. *IEEE Control Syst. Mag.* **2016**, *36*, 59–82.
10. Ghommam, J.; Mehrjerdi, H.; Saad, M.; Mnif, F. Formation path following control of unicycle-type mobile robots. *Robot. Auton. Syst.* **2010**, *58*, 727–736. [CrossRef]
11. Reyes, L.A.V.; Tanner, H.G. Flocking, formation control, and path following for a group of mobile robots. *IEEE Trans. Control Syst. Technol.* **2014**, *23*, 1268–1282. [CrossRef]
12. Jiang, H.; Xiong, B.; Zhang, H.; Basar, E. Physics-Based 3D End-to-End Modeling for Double-RIS Assisted Non-Stationary UAV-to-Ground Communication Channels. *IEEE Trans. Commun.* **2023**, *71*, 4247–4261. [CrossRef]
13. Wu, B.; Zhang, B.; Guo, D.; Wang, H.; Jiang, H. Anti-jamming trajectory design for UAV-enabled wireless sensor networks using communication flight corridor. *China Commun.* **2022**, *19*, 37–52. [CrossRef]
14. Frew, E.W.; Lawrence, D.A.; Morris, S. Coordinated Standoff Tracking of Moving Targets Using Lyapunov Guidance Vector Field. *J. Guid. Control. Dyn.* **2008**, *31*, 290–306. [CrossRef]
15. Lawrence, D.A.; Frew, E.; Pisano, W.J. Lyapunov Vector Fields for Autonomous UAV Flight Control. In Proceedings of the AIAA Navigation and Control Conference and Exhibit, Hilton Head, SC, USA, 20–23 August 2007.
16. Summers, T.H.A.; Mears, M.R. Coordinated standoff tracking of moving targets: Control laws and information architectures. *J. Guid. Control Dyn.* **2008**, *32*, 56–69. [CrossRef]
17. Nakai, K.; Uchiyama, K. Vector Fields for UAV Guidance Using Potential Function Method for Formation Flight. In Proceedings of the AIAA Guidance, Navigation, and Control (GNC) Conference, Boston, MA, USA, 19–22 August 2013.
18. Hyondong, O.; Seungkeun, K.; Antonios, T.; White, B.A. Decentralised standoff tracking of moving targets using adaptive sliding mode control for UAVs. *J. Intell. Robot. Syst.* **2014**, *76*, 169–183.
19. Gonçalves, V.M.; Pimenta, L.C.; Maia, C.A.; Pereira, G.A. Coordination of multiple fixed-wing UAVs traversing intersecting periodic paths. In Proceedings of the 2013 IEEE International Conference on Robotics and Automation, Karlsruhe, Germany, 6–10 May 2013; pp. 849–854.
20. Xargay, E.; Kaminer, I.; Pascoal, A.; Hovakimyan, N.; Dobrokhodov, V.; Cichella, V.; Aguiar, A.P.; Ghabcheloo, R. Time-critical cooperative path following of multiple unmanned aerial vehicles over time-varying networks. *J. Guid. Control Dyn.* **2013**, *36*, 499–516. [CrossRef]
21. Wang, Y.; Wang, D.; Zhu, S. Cooperative moving path following for multiple fixed-wing unmanned aerial vehicles with speed constraints. *Automatica* **2019**, *100*, 82–89. [CrossRef]
22. Fang, X.; Xie, L. Distributed Formation Maneuver Control Using Complex Laplacian. *IEEE Trans. Autom. Control* **2024**, *69*, 1850–1857. [CrossRef]

23. Li, K.; Shen, Z.; Jing, G.; Song, Y. Angle-constrained formation control under directed non-triangulated sensing graphs. *Automatica* **2024**, *163*, 111565. [CrossRef]
24. Yang, Y.; Wang, X.; Daldi, S.; Singh, S.; Fari, S. A soflware-in-the-Loop Implementation of Adaptive Formation Control for Fixed-Wing UAVs. *IEEE/CAA J. Autom. Sin.* **2019**, *6*, 1230–1239. [CrossRef]
25. Yao, W.; de Marina, H.G.; Sun, Z.; Cao, M. Distributed coordinated path following using guiding vector fields. In Proceedings of the 2021 IEEE International Conference on Robotics and Automation (ICRA), Xi'an, China, 30 May–5 June 2021; pp. 10030–10037.
26. Pham, T.V.; Vu, D.V.; Nguyen, D.T.; Dong, N.N. Cooperative Path-Following Control of Fixed-Wing UAV Swarm under Communication Delay. In Proceedings of the 2023 IEEE/AIAA 42nd Digital Avionics Systems Conference (DASC), Barcelona, Spain, 1–5 October 2023; pp. 1–5. [CrossRef]
27. McLain, B.T.W. *Small Unmanned Aircraft: Theory and Practice*; Princeton University Press: Princeton, NJ, USA, 2012.
28. Pham, T.V.; Vu, D.V.; Nguyen, D.T.; Dong, N.N. Loitering Formation of Fixed-Wing UAV Swarm under Communication Delay and Switching Topology. *IFAC-PapersOnLine* **2023**, *56*, 8512–8517. [CrossRef]
29. Buslowicz, M. Simple stability criterion for a class of delay differential systems. *Int. J. Syst. Sci.* **1987**, *18*, 993–995. [CrossRef]
30. Pham, T.V.; Thanh Nguyen, Q.T.; Messai, N.; Manamanni, N. Output consensus design in clustered networks of heterogeneous linear MASs under disturbances. *Eur. J. Control* **2023**, *69*, 100726. [CrossRef]